Available online at www.sciencedirect.com

ScienceDirect

Procedia IUTAM 00 (2011) 1–20

Procedia IUTAM

www.elsevier.com/locate/procedia

Bridging Scales with a Generalized Finite Element Method

J. Garzon[a], V. Gupta[a], A. Simone[b], C.A. Duarte[a,*]

[a]*Department of Civil and Environmental Engr., University of Illinois at Urbana-Champaign, Newmark Laboratory, 205 North Mathews Avenue, Urbana, Illinois 61801, USA*
[b]*Faculty of Civil Engineering and Geosciences, Delft University of Technology P.O. Box 5048, 2600 GA Delft, The Netherlands*

Abstract

The generalized FEM (GFEM) has been successfully applied to the simulation of dynamic propagating fractures, polycrystalline and fiber-reinforced microstructures, porous materials, etc. A-priori knowledge about the solution of these problems are used in the definition of their GFEM approximation spaces. This leads to more accurate and robust simulations than available finite element methods while relaxing some meshing requirements. This is demonstrated in a simulation of intergranular crack propagation in a brittle polycrystal using simple background meshes.

For many classes of problems – like those with material non-linearities or involving multiscale phenomena – a-priori knowledge of the solution behavior is limited. In this paper, we present a GFEM based on the solution of interdependent global (structural) and fine-scale or local problems. The local problems focus on the resolution of fine-scale features of the solution in the vicinity of, e.g., evolving fracture process zones while the global problem addresses the macro-scale structural behavior. Fine-scale solutions are accurately solved using an *hp*-adaptive GFEM and thus the proposed method does not rely on analytical solutions. These solutions are embedded into the global solution space using the partition of unity method. This GFEM enables accurate modeling of problems involving multiple scales of interest using meshes with elements that are orders of magnitude larger than those required by the FEM. Numerical examples illustrating the application of this class of GFEM to high-cycle fatigue crack growth of small cracks and to problems exhibiting localized non-linear material responses are presented.

Keywords:
Generalized Finite Element Method, Extended Finite Element Method, Multiscale, Polycrystals, Fracture, Crack Growth, Global-Local Analysis

1. Introduction

Many problems of engineering relevance exhibit strongly interacting multiscale effects. Their modeling and simulation demand analytical and computational tools that do not assume a view of nature that partitions phenomena into categories of scales [1]. One example of particular interest – and which is part of the motivation behind this work – lies in the structural analysis of stealth aircrafts. To increase the stealthiness

*Department of Civil and Environmental Engineering, University of Illinois at Urbana-Champaign
2122 Newmark Laboratory MC 250, 205 North Mathews Av., Urbana, Illinois 61801, USA
Email address: caduarte@illinois.edu (C.A. Duarte)
URL: http://netfiles.uiuc.edu/caduarte/www/ (C.A. Duarte)

of aircrafts like the one shown in Figure 1, a high temperature panel is used at the exhausts of the embedded engines. These panels are subjected to an intense thermo-mechanical-acoustic environment and can fail in high-cycle fatigue due to the acoustic and vibration loading, in low-cycle fatigue due to thermal and mechanical loading, and by material degradation or oxidation due to the extreme thermal environment [2]. Experiments in these environments are difficult, limited and extremely costly.

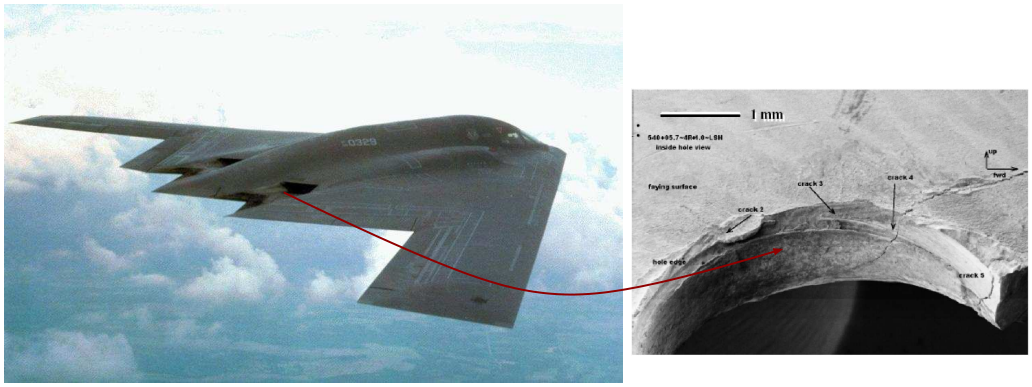

Fig. 1. Micro-crack growth in structures subjected to intense thermo, mechanical and acoustic loads involves complex interactions over vastly different scales [http://media.defenseindustrydaily.com/images/].

The analysis of this class of problems with the FEM requires extremely refined meshes. This may create severe restrictions in maximum time step allowed for accurate time integration of the solution [2, 3]. Dynamic load balancing for efficient parallel computations becomes quite challenging for this type of discretization [3]. In addition, the construction of properly adapted discretizations can be quite costly since it demands several adaptive cycles on large computational models. Another severe issue with a Direct Numerical Simulation (DNS) approach based on available methods is the ill-conditioning of the resulting system of equations [4] due to the extremely large ratio between element sizes in the FEM mesh. One workaround for this issue is to perform the computations using high-precision 128-bit floating-point arithmetic [3]. However, few compilers or software libraries can handle high-precision arithmetic, and those that do so are extremely slow – often 50 to 100 times slower than conventional 64-bit floating-point arithmetic [3].

The generalized FEM [5, 6, 7, 8, 9] is an instance of the so-called partition of unity method which has its origins in the works of Babuška *et al.* [10, 6, 11] and Duarte and Oden [12, 13, 14, 15, 8]. The extended FEM [16, 17] and several other methods proposed in recent years can also be formulated as special cases of the partition of unity method. Recent reviews of G/XFEM can be found in [18, 19]. The partition of unity in the Generalized FEM (GFEM) is provided by low order Lagrangian finite element shape functions. These functions are combined with local function approximation spaces built around a-priori knowledge about the solution of a given problem. These functions provide more accurate and robust simulations than the polynomial functions traditionally used in the standard FEM while relaxing some meshing requirements of the FEM. An example of this class of GFEM based on analytically derived local spaces is the GFEM for polycrystals proposed in [20]. In this GFEM, discretization of polycrystalline micro-structures requires only a simple background mesh on which the polycrystalline topology is superimposed.

In many classes of problems – like those involving multiscale phenomena or material non-linearities – local approximation spaces are, in general, not amenable to analytical derivation. To overcome this limitation, basis functions for these spaces are defined from the numerical solution of boundary-value problems. Section 4 summarizes the so-called Generalized Finite Element with global-local enrichments (GFEM^{gl}). In this method, basis functions are numerically defined using concepts from the classical global-local finite element method [21, 22, 23, 24] and a multiscale decomposition of the solution of a boundary or initial value problem is performed. The coarse scale component of the solution is approximated by discretizations defined on coarse finite element meshes. The fine-scale component is, in turn, approximated by the solution of local problems defined in neighborhoods of regions exhibiting multiscale effects such as in the neighbor-

hood of micro-cracks. Boundary conditions for the local problems are provided by the available solution at a crack growth step. The methodology enables accurate modeling of, e.g., 3-D propagating cracks on meshes with elements that are orders of magnitude larger than those required by the FEM. The coarse-scale mesh remains unchanged during the simulation. This, combined with the hierarchical nature of GFEM shape functions, leads to significant computational savings when compared with a DNS approach [25].

A related method aimed at modeling interactions among multiple static cracks is the multiscale method of Loehnert and Belytschko [26]. Other related methods for two-dimensional static cracks include the spider-XFEM [27] and the reduced basis enrichment for the XFEM [28] of Chahine et al.; the method of Menk and Bordas for fracture of bi-material systems [29]; the harmonic enrichment functions of Mousavi et al. [30] for two-dimensional branched cracks.

The outline of this paper is as follows. Section 2 summarizes the main ingredients of GFEM approximation spaces. The GFEM for polycrystals is reviewed in Section 3 and an application of this method to the simulation of intergranular crack propagation in a brittle polycrystal is presented in Section 5.1. The formulation of a GFEM^{gl} for 3-D crack growth is presented in Section 4. Numerical examples illustrating the application of this class of GFEM to high-cycle fatigue crack growth of small cracks and to problems exhibiting localized non-linear material responses are presented in Sections 5.2 and 5.3. The main conclusions are outlined in Section 6.

2. The Generalized Finite Element Method

A GFEM approximation space (i.e., a trial space) is based on three components: (a) patches or clouds, (b) a partition of unity, and (c) local approximation spaces. We describe these components as follows:

(a) *Patches or Clouds* ω_α: In the generalized finite element method, a cloud ω_α is given by the union of the finite elements sharing node α of the finite element mesh covering the domain of interest Ω. The set $\{\omega_\alpha\}_{\alpha=1}^N$, in a finite element mesh with N nodes, is an open cover of Ω, i.e.,

$$\Omega = \cup_{\alpha=1}^N \omega_\alpha.$$

(b) *Partition of Unity Subordinate to the Cover* $\{\omega_\alpha\}_{\alpha=1}^N$: The Lagrangian finite element shape functions $\varphi_\alpha,\ \alpha = 1, \ldots, N$, constitute a partition of unity, i.e., $\sum_{\alpha=1}^N \varphi_\alpha(\boldsymbol{x}) = 1$ for all $\boldsymbol{x}$ in Ω. This is a key property used in partition of unity methods.

(c) *Cloud or Patch Approximation Spaces* χ_α: To each patch ω_α, we associate an m_α-dimensional space χ_α of functions defined on ω_α, namely,

$$\chi_\alpha = \mathrm{span}\{L_{\alpha i},\ 1 \le i \le m_\alpha,\ L_{\alpha i} \in H^1(\omega_\alpha)\}.$$

The basis functions $L_{\alpha i}$ above are also known as *enrichment functions*.

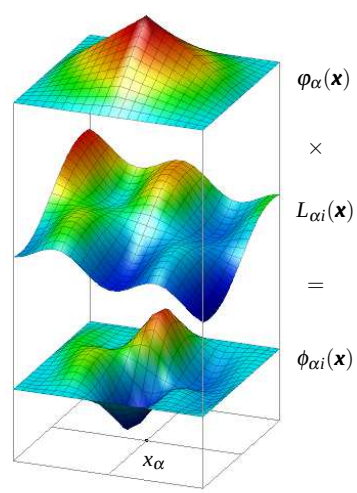

Fig. 2. The generalized FEM shape function $\phi_{\alpha i}$ at x_α is constructed by considering the product of the Lagrangian finite element shape function φ_α and the non-polynomial enrichment $L_{\alpha i}$.

The trial space for the GFEM is given by

$$S^{GFEM}(\Omega) \equiv \sum_{\alpha=1}^{N} \varphi_\alpha \chi_\alpha = \mathrm{span}\{\phi_{\alpha i} := \varphi_\alpha L_{\alpha i},\ 1 \le i \le m_\alpha,\ 1 \le \alpha \le N\}.$$

The function

$$\phi_{\alpha i}(\boldsymbol{x}) = \varphi_\alpha(\boldsymbol{x}) L_{\alpha i}(\boldsymbol{x}) \qquad \text{(no summation on } \alpha\text{)}, \tag{1}$$

where α is a node in the finite element mesh, is called a GFEM shape function. Figure 2 illustrates the construction of GFEM shape functions in a two-dimensional domain.

The enrichment functions in χ_α are chosen carefully to mimic the properties of the function to be approximated locally in ω_α. This is often done by using the available information on the approximated function. Choosing suitable patch spaces for a particular problem is central to the approximation property of GFEM.

3. A GFEM for Polycrystals

The GFEM for polycrystals [20] is illustrated in Figure 3. Discretization of polycrystalline microstructres with this method requires only a simple background mesh on which the polycrystalline topology is superimposed. Grain boundaries and junctions can be arbitrarily located within elements. The main concepts used in this GFEM are summarized. Details can be found in [20].

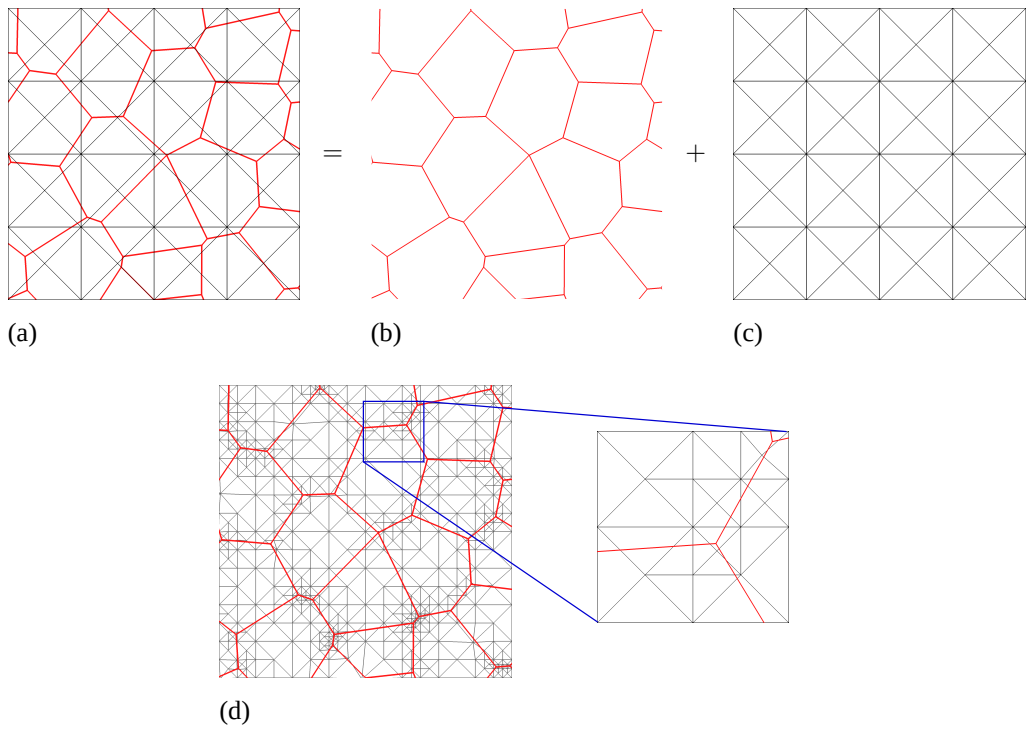

Fig. 3. In the GFEM for polycrystals (a), a polycrystalline aggregate is described by superimposing a polycrystalline topology (b) on a background mesh (c). The quality of the numerical solution can be improved by local mesh refinement (d). Note that the finite element mesh does not conform to grain boundaries and junctions.

Consider the following decomposition of the displacement field $\boldsymbol{u}$ of a polycrystal comprising $N_{\mathcal{G}}$ grains

$$\boldsymbol{u} = \hat{\boldsymbol{u}} + \sum_{j=1}^{N_{\mathcal{G}}} \mathcal{H}_j \tilde{\boldsymbol{u}}_j, \tag{2}$$

where the generalized $\mathcal{H}_j$ function is equal to 1 in grain j and 0 otherwise. Enrichment functions, $L_{\alpha i}$, used at node α are taken as the set of functions $\mathcal{H}_j$ that are discontinuous on cloud ω_α [20]. A traction-separation law is used at grain boundaries and a constitutive relationship describing the material behavior is adopted within the grains. An application of this method to the simulation of intergranular crack propagation in a brittle polycrystal is presented in Section 5.1. It is to be noted that the method is capable of describing more complex failure scenario with combined transgranular and intergranular cracking, provided rules for the transition from one type to the other are defined.

4. GFEM^{gl}: Bridging Scales with Global-Local Enrichment Functions

Global-local enrichment functions can be defined for many classes of problems like interacting 3-D cracks [31], propagating 3-D fractures [25] or problems exhibiting sharp thermal gradients [32, 33]. These functions can also be developed for problems involving localized non-linear material responses [34]. They are able to represent fine-scale responses on *coarse*, macroscale, finite element meshes and to fully account for interactions among scales. Detailed mathematical analysis of this class of GFEM is presented in [35, 36].

In this section, we consider the case of 3-D simulations of propagating mechanically-short cracks. These cracks are much smaller than any dimension of a structural component but larger than the details of the material micro-structure [37].

4.1. Problem Formulation

Consider a domain $\Omega \subset \mathbb{R}^3$. The boundary $\partial\Omega$ is decomposed as $\partial\Omega = S^u \cup S^f$ with $S^u \cap S^f = \emptyset$. The equilibrium equations are given by

$$\nabla \cdot \boldsymbol{\sigma} = \mathbf{0} \qquad \text{in } \Omega. \tag{3}$$

The following boundary conditions are prescribed on $\partial\Omega$:

$$\boldsymbol{\sigma} \cdot \boldsymbol{n} = \bar{\boldsymbol{t}} \ \text{ on } S^f, \qquad \boldsymbol{\sigma} \cdot \boldsymbol{n} = \eta(\bar{\boldsymbol{u}} - \boldsymbol{u}) \ \text{ on } S^u, \tag{4}$$

where $\boldsymbol{n}$ is the outward unit normal vector to $\partial\Omega$ and $\bar{\boldsymbol{t}}$ are prescribed tractions. The second equation represents a spring or Robin boundary condition [38]: η is the stiffness of the spring, $\bar{\boldsymbol{u}}$ is displacement imposed at the base of the spring system and $\boldsymbol{u}$ is the displacement at the boundary of the body. Dirichlet boundary conditions can be treated as a limiting case of this type of boundary conditions [38].

The constitutive relations may be given by the generalized Hooke's law, $\boldsymbol{\sigma} = \boldsymbol{C} : \boldsymbol{\varepsilon}$, where $\boldsymbol{C}$ is Hooke's tensor, or by a non-linear stress-strain relation. In this case, the classical rate-independent J_2 flow theory for small strains with isotropic hardening is adopted. The weak formulation of the problem described above is given by:

Find $\boldsymbol{u} \in H^1(\Omega)$, such that $\forall\, \boldsymbol{v} \in H^1(\Omega)$

$$\int_\Omega \boldsymbol{\sigma}(\boldsymbol{u}) : \boldsymbol{\varepsilon}(\boldsymbol{v}) d\Omega + \eta \int_{S^u} \boldsymbol{u} \cdot \boldsymbol{v} dS = \int_{S^f} \bar{\boldsymbol{t}} \cdot \boldsymbol{v} dS + \eta \int_{S^u} \bar{\boldsymbol{u}} \cdot \boldsymbol{v} dS, \tag{5}$$

where $H^1(\Omega)$ is a Hilbert space defined on Ω.

4.2. Computation of Global-Local Enrichments: Coarse-Scale Problem at Simulation Step t

Let $\boldsymbol{u}_G^t$ denote a generalized FEM approximation of the Problem (5) at damage evolution (or load) step t. This approximation is the solution of the following global problem:

Find $\boldsymbol{u}_G^t \in \boldsymbol{S}_G^{GFEM,t}(\Omega) \subset H^1(\Omega)$ such that, $\forall\, \boldsymbol{v}_G^t \in \boldsymbol{S}_G^{GFEM,t}(\Omega)$

$$\int_\Omega \boldsymbol{\sigma}(\boldsymbol{u}_G^t) : \boldsymbol{\varepsilon}(\boldsymbol{v}_G^t) d\Omega + \eta \int_{S^u} \boldsymbol{u}_G^t \cdot \boldsymbol{v}_G^t dS = \int_{S^f} \bar{\boldsymbol{t}}^t \cdot \boldsymbol{v}_G^t dS + \eta \int_{S^u} \bar{\boldsymbol{u}}^t \cdot \boldsymbol{v}_G^t dS, \tag{6}$$

where $\boldsymbol{S}_G^{GFEM,t}(\Omega) \subset H^1(\Omega)$ is the generalized FEM space at simulation step t. The enrichment functions in $\boldsymbol{S}_G^{GFEM,t}(\Omega)$ are defined in local spaces and *have to be computed on-the-fly*. We describe a fine-scale problem in the next subsection to achieve this goal. The mesh used to solve Problem (6) is typically a *coarse*, quasi-uniform mesh, *regardless of the presence of cracks or localized non-linear responses in the domain*. Figure 4 illustrates one such discretization. Problem (6) leads to a system of non-linear equations for the unknown degrees of freedom of $\boldsymbol{u}_G^t$.

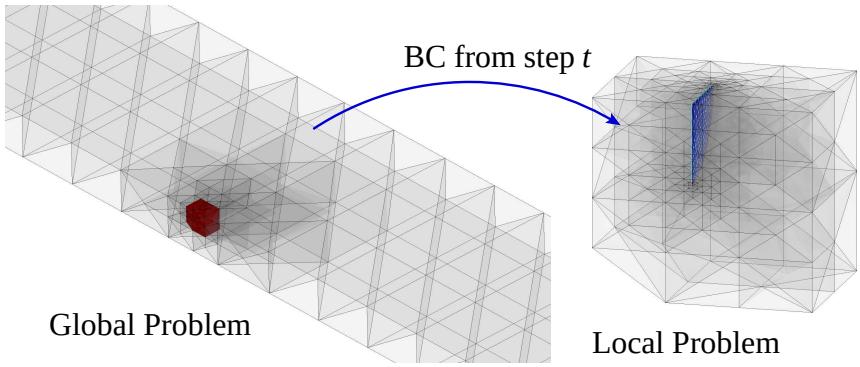

Fig. 4. Illustration of the GFEM^{gl} for crack propagation. The figure shows the neighborhood Ω_L of a small propagating crack in the global domain. The solution of the global problem at simulation step t provides boundary conditions for the extracted local domain.

4.3. Computation of Global-Local Enrichments: Fine-Scale Problems at Simulation Step t

The GFEM^{gl} involves the solution of a fine-scale boundary value problem defined at a neighborhood Ω_L of a fine-scale feature like the crack shown in Figure 4. Having the global approximation $\boldsymbol{u}_G^t$ at simulation step t, the following fine-scale problem on Ω_L is solved to find enrichment functions for the space $\boldsymbol{S}_G^{GFEM,t+1}(\Omega)$:

Find $\boldsymbol{u}_L^t \in \boldsymbol{S}_L^{GFEM,t}(\Omega_L) \subset H^1(\Omega_L)$, such that $\forall\ \boldsymbol{v}_L^t \in \boldsymbol{S}_L^{GFEM,t}(\Omega_L)$

$$\begin{aligned}&\int_{\Omega_L} \boldsymbol{\sigma}(\boldsymbol{u}_L^t) : \boldsymbol{\varepsilon}(\boldsymbol{v}_L^t) d\Omega + \eta \int_{\partial\Omega_L \cap S^u} \boldsymbol{u}_L^t \cdot \boldsymbol{v}_L^t dS + \kappa \int_{\partial\Omega_L \setminus (\partial\Omega_L \cap \partial\Omega)} \boldsymbol{u}_L^t \cdot \boldsymbol{v}_L^t dS \\ &= \int_{\partial\Omega_L \cap S^f} \overline{\boldsymbol{t}}^t \cdot \boldsymbol{v}_L^t dS + \eta \int_{\partial\Omega_L \cap S^u} \overline{\boldsymbol{u}}^t \cdot \boldsymbol{v}_L^t dS + \int_{\partial\Omega_L \setminus (\partial\Omega_L \cap \partial\Omega)} \left(\boldsymbol{t}(\boldsymbol{u}_G^t) + \kappa \boldsymbol{u}_G^t\right) \cdot \boldsymbol{v}_L^t dS, \end{aligned} \tag{7}$$

where $\boldsymbol{S}_L^{GFEM,t}(\Omega_L)$ is a discretization of $H^1(\Omega_L)$ using GFEM shape functions presented in [39].

A key aspect of Problem (7) is the use of the coarse-scale solution at simulation step t, $\boldsymbol{u}_G^t$, to compute the boundary condition on $\partial\Omega_L \setminus (\partial\Omega_L \cap \partial\Omega)$. The numerical nature of the coarse-scale solution used for the fine-scale boundary conditions leads to the use of the terminology "inexact boundary conditions". Exact boundary conditions are prescribed on portions of $\partial\Omega_L$ that intersect either S^u or S^f. The traction vector, $\boldsymbol{t}(\boldsymbol{u}_G^t)$, that appears in the integral over $\partial\Omega_L \setminus (\partial\Omega_L \cap \partial\Omega)$ can be computed using,

$$\boldsymbol{t}(\boldsymbol{u}_G^t) = \hat{\boldsymbol{n}} \cdot \boldsymbol{\sigma}(\boldsymbol{u}_G^t) \tag{8}$$

where $\hat{\boldsymbol{n}}$ is the outward unit normal vector to $\partial\Omega_L$. The spring stiffness, κ, can be selected using [34, 40]

$$\kappa = \frac{E}{\sqrt[nd]{V_0 J}}, \tag{9}$$

where E is the Young's modulus, nd is the number of spatial dimensions of the problem, V_0 is the volume of the master element used and J is the Jacobian of the global element across the local boundary where the spring boundary condition is imposed.

4.4. Scale-Bridging with Global-Local Enrichment Functions

The solution, $\boldsymbol{u}_L^t$, of the fine-scale problem defined above is used to build generalized FEM shape functions

$$\boldsymbol{\phi}_\alpha^{t+1}(\boldsymbol{x}) := \varphi_\alpha(\boldsymbol{x}) \boldsymbol{u}_L^t(\boldsymbol{x}) \tag{10}$$

defined on the coarse-scale (global) mesh, where the partition of unity function, φ_α, is provided by a global, *coarse*, FE mesh and $\boldsymbol{u}_L^t$ has the role of an enrichment or basis function for the patch space $\chi_\alpha(\omega_\alpha)$. Hereafter,

$\boldsymbol{u}_L^t$ is denoted as a *global-local enrichment function*. The global GFEM space containing shape functions $\boldsymbol{\phi}_{\alpha i}^{t+1}$ is denoted $\boldsymbol{S}_G^{GFEM,t+1}(\Omega)$ and is given by

$$\boldsymbol{S}_G^{GFEM,t+1}(\Omega) = \left\{ \boldsymbol{u}^{hp} = \underbrace{\sum_{\alpha=1}^{N_G} \sum_{i=1}^{D_\alpha} \varphi_\alpha(\boldsymbol{x})\, \underline{\boldsymbol{u}}_{\alpha i} L_{\alpha i}(\boldsymbol{x})}_{\text{global approx.}} + \underbrace{\sum_{\beta \in \mathcal{I}_{gl}^{t+1}} \varphi_\beta(\boldsymbol{x}) \boldsymbol{u}_\beta^{gl(t)}(\boldsymbol{x})}_{\text{local approx.}} \right\}, \tag{11}$$

where $\mathcal{I}_{gl}^{t+1}$ is the index set of nodes enriched at simulation step $t+1$ with function $\boldsymbol{u}_L^t$ computed at (7) and

$$\boldsymbol{u}_\beta^{gl(t)}(\boldsymbol{x}) = \begin{bmatrix} \underline{u}_{\beta 1}^{gl}\, u_{L1}^t(\boldsymbol{x}) \\ \underline{u}_{\beta 2}^{gl}\, u_{L2}^t(\boldsymbol{x}) \\ \underline{u}_{\beta 3}^{gl}\, u_{L3}^t(\boldsymbol{x}) \end{bmatrix},$$

where $\underline{u}_{\beta j}^{gl}$, $\beta \in \mathcal{I}_{gl}^{t+1}$, $j = 1,2,3$, are nodal degrees of freedom, and $u_{Lj}^t(\boldsymbol{x})$, $j = 1,2,3$, are the Cartesian components of displacement vector $\boldsymbol{u}_L^t$.

The coarse-scale Problem (6) is solved for $\boldsymbol{u}_G^{t+1} \in \boldsymbol{S}_G^{GFEM,t+1}(\Omega)$ and the procedure is repeated at each damage (or load) evolution step. The hierarchical enrichment of the coarse global mesh with a fine-scale solution is illustrated in Figure 5.

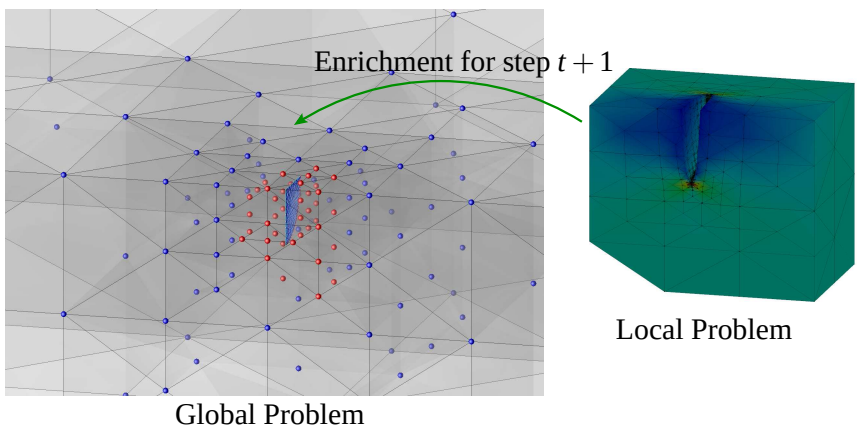

Fig. 5. Hierarchical enrichment of the coarse global mesh with local solutions computed on locally refined mesh. Only three degrees of freedom are added to these global nodes (shown with red spheres in the global mesh). These enrichments are used to approximate the global solution in the neighborhood of the crack at simulation step $t+1$.

5. Numerical examples

5.1. Intergranular crack propagation

In this section we analyze intergranular brittle cracking of a polycrystalline aggregate by means of the GFEM for polycrystals with cohesive grain boundaries and linear elastic grains. The geometry and boundary conditions of the problem are shown in Figure 6. The notched specimen is loaded by a uniform tensile stress, σ, which is varied incrementally under quasi-static loading conditions.

An 80 grain polycrystalline microstructure is used inside the process zone depicted in Figure 6. The process zone is the region in which grains and grain boundaries are represented explicitly; outside this zone the material is a homogeneous continuum. The aggregate realization considered in this study was generated

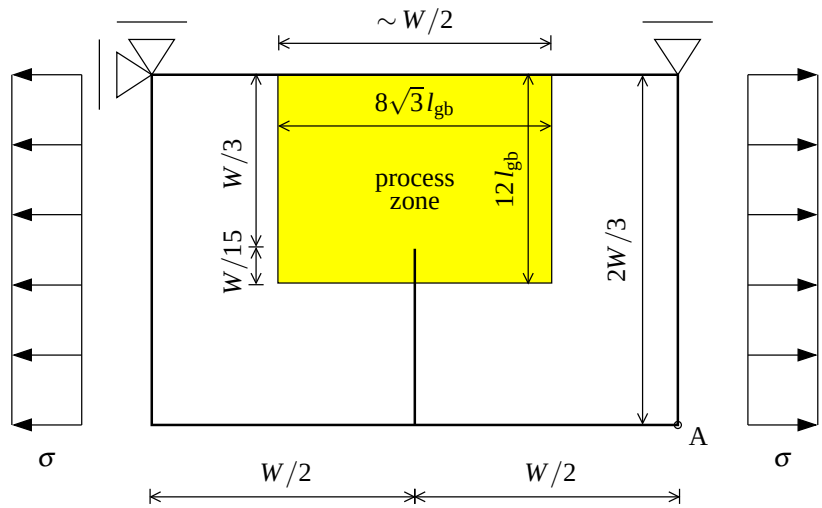

Fig. 6. Geometry and boundary conditions for the notched specimen employed in the simulations.

using a centroidal Voronoi tessellation algorithm. The average grain size is approximately 21 μm which corresponds to an average grain-boundary length $l_{gb} \approx 12\,\mu$m. Since there are 80 grains in the process zone, the length of the specimen is $W = 360\,\mu$m.

The material parameters are taken to be representative of an average polycrystalline alumina, Al_2O_3. We assume the grains to be elastic and isotropic, with Young's modulus $E = 384.6$ GPa and Poisson's ratio $\nu = 0.237$. Plane strain conditions and small elastic strains and rotations are assumed.

Non-linearity in the material response is defined by the cohesive law across grain boundaries. In this study, we have used the Xu-Needleman cohesive law [41]. The following parameters for this law are adopted: critical fracture energy $G_{Ic} = 39.3$ J/m^2 and grain boundary cohesive strength $\sigma_{max} = 0.6$ GPa.

The partition of unity adopted in this section is provided by constant strain triangles. The elements that intersect the grain boundaries are refined to the desired level as illustrated in Figure 3. Since the mesh does not have to fit the aggregate geometry, mesh refinement preserves the aspect ratio of the elements [42]. The refinement level for acceptable accuracy is governed by the size of the fracture process zone along the grain boundaries as discussed in [43].

Figure 7 shows the aggregate topology near the crack tip. The figure also shows the GFEM discretization of the aggregate and the computed crack path. The contour plot represents the normalized von Mises equivalent stress. Note that the finite element mesh does not conform to grain boundaries and junctions. Thus mesh generation issues faced by the FEM do not exist in the GFEM. Therefore, a large number of randomly generated polycrystalline aggregates can be automatically analyzed [43].

The boundary conditions shown in Figure 6 promote and achieve mode-I cracking at the specimen level. However, as shown in Figure 7, local failure at the grain-boundary level is dictated by the granular arrangement and exhibits both mode-I and mode-II cracking [43].

5.2. Analysis of three-dimensional cracks

This section presents two applications of the GFEM^{gl} described in Section 4. The first one deals with a static quarter penny-shaped crack as illustrated in Figure 8. This problem is used in the verification of the method using as reference the solutions by Raju and Newman [44] and Ali [45] for corner cracks. The second problem deals with the propagation of a small corner crack in a plate subjected to a cyclic load. In both cases, polynomial enrichments of degree $p = 3$ is adopted at global and local problems.

5.2.1. Quarter penny-shaped crack

The problem consists of a quarter penny-shaped crack located at the corner of a plate subjected to a uniform tensile load σ at its ends (cf. Figure 8). Displacement constraints are also imposed near the ends

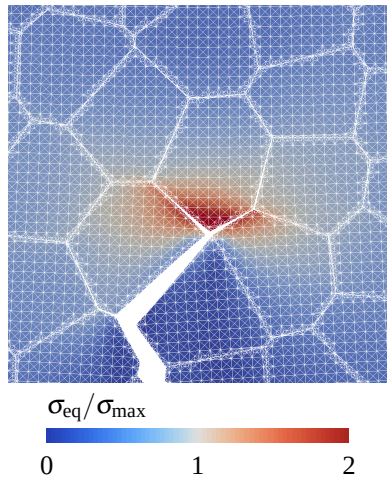

Fig. 7. Failure characterization in brittle polycrystals with the GFEM: intergranular cracking (20 × displacement magnification) and normalized von-Mises equivalent stress. Note that a uniform FEM mesh was used in the computation —the figure also shows sub-element used for integration of the weak form over finite elements cut by grain boundaries.

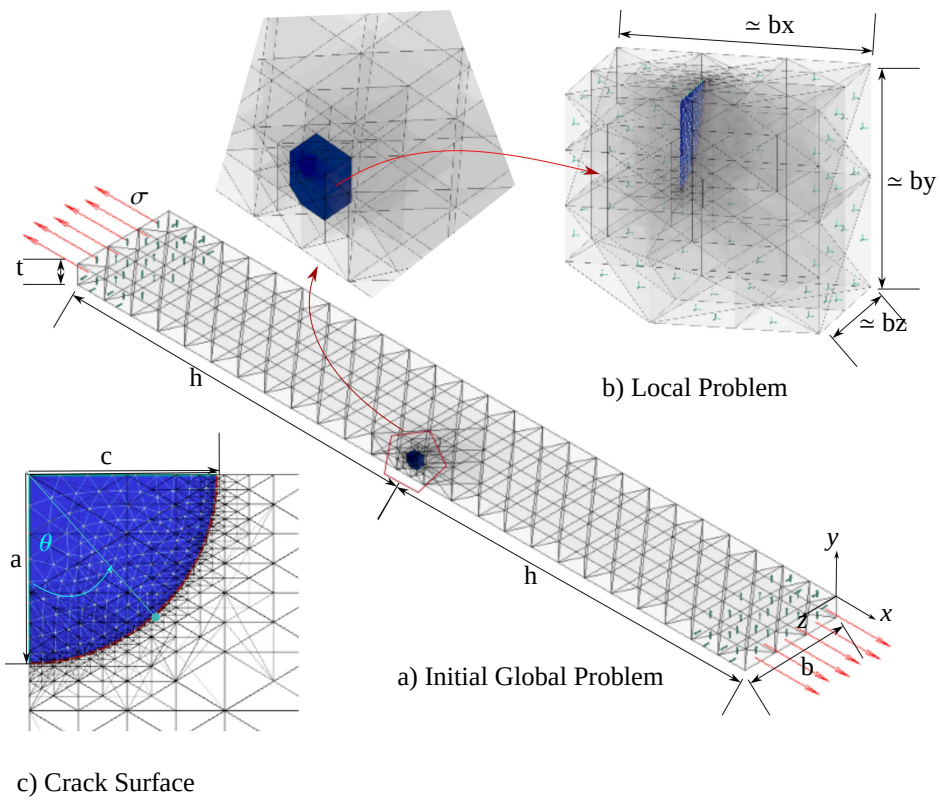

Fig. 8. Corner-cracked plate problem subjected to tensile axial load.

of the plate in order to minimize rotations under the applied loads. In this problem we consider a quarter circular crack and thus, in Figure 8c, $a = c$. In the case of static cracks, the first step in the GFEM^{gl} involves the solution of the global problem on a mesh enriched with polynomial functions only. Thus, no cracks are considered at this stage. This problem is hereafter denoted as the *initial global problem*. This is illustrated

in Figure 8a. The global mesh is quasi-uniform while in the local problem the mesh is strongly refined at the crack front. The ratio between the element size at the crack front, L_e^L, and the crack size, a, is taken as $L_e^L/a \simeq 0.03$. The ratio between the size of the smallest element in the mesh of the global problem, L_e^G, and the crack size, a, is $L_e^G/a = 0.5$. Note that in the GFEM^{gl}, cracks are not explicitly discretized in the global problem. Instead, they are represented through global-local enrichments, i.e. the solution of local problems. Thus, the global mesh does not change during a simulation. The following dimensions are adopted for the plate: $2h/c = 180.5$, $a/t = 0.2$ and $a/b = 0.04$.

Figure 8b shows the local problem where the crack is discretized using analytically defined enrichment functions as described in [39]. The size of the local domain is significantly smaller than the global one. The local domain is defined by global elements contained in a bounding box with dimensions $bx/a = 2$, $by/a = 2$, $bz/a = 2$ in the $x-$, $y-$ and $z-$ directions, respectively. The size of the local domain is about 2% of the original problem size.

The solution of the global problem enriched with global-local functions is shown in Figure 9. This problem is hereafter denoted as the *enriched global problem*. The global mesh is quite coarse and yet it can capture the singularity at the crack front.

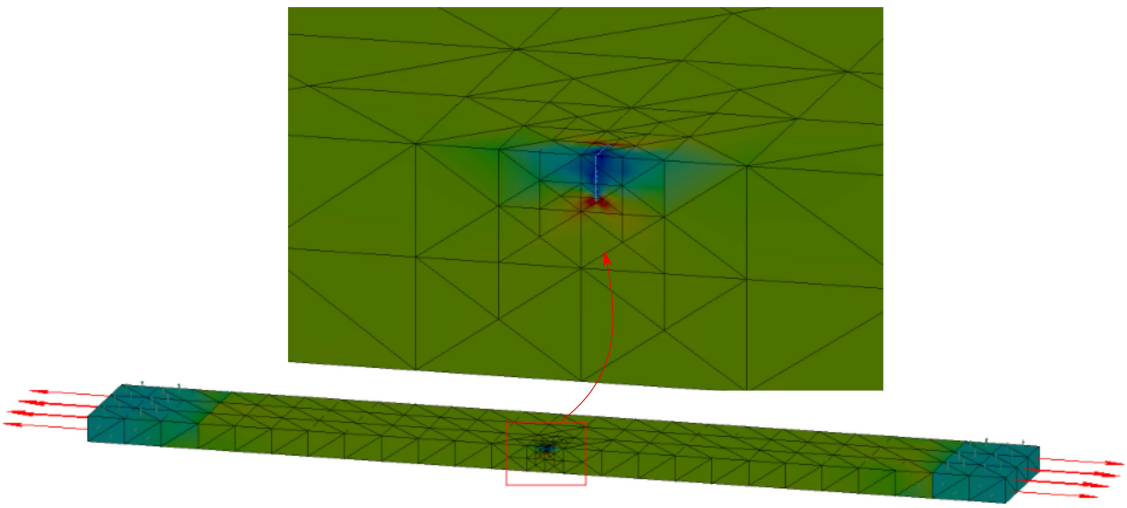

Fig. 9. Enriched global problem solution.

Figure 10 shows the normalized mode I stress intensity factor K_I/K_r extracted from the solution of the enriched global and local problems. They are denoted as GFEM^{gl} and GL-FEM in the figure, respectively. K_I was extracted using a formulation of the Cut-Off Function Method [38] adapted for the GFEM [46, 47, 48]. The reference solutions by Raju and Newman [44] and Ali [45] are also shown. The horizontal axis in the figure denotes the angular position at the crack front as illustrated in Figure 8c. The normalizing factor, K_r, is taken as

$$K_r = \sigma \sqrt{\frac{\pi a}{Q}} \tag{12}$$

with Q

$$Q = 1 + 1.464\left(\frac{a}{c}\right)^{1.65}. \tag{13}$$

The example presented in this section shows that Stress Intensity Factors (SIFs) extracted from the GFEM^{gl} solution are significantly more accurate than those extracted from the local solution and agrees very well with the reference solutions. The local solution is equivalent to one provided by a global-local FEM analysis, which is commonly used in the industry to handle problems involving multiple spatial scales of interest.

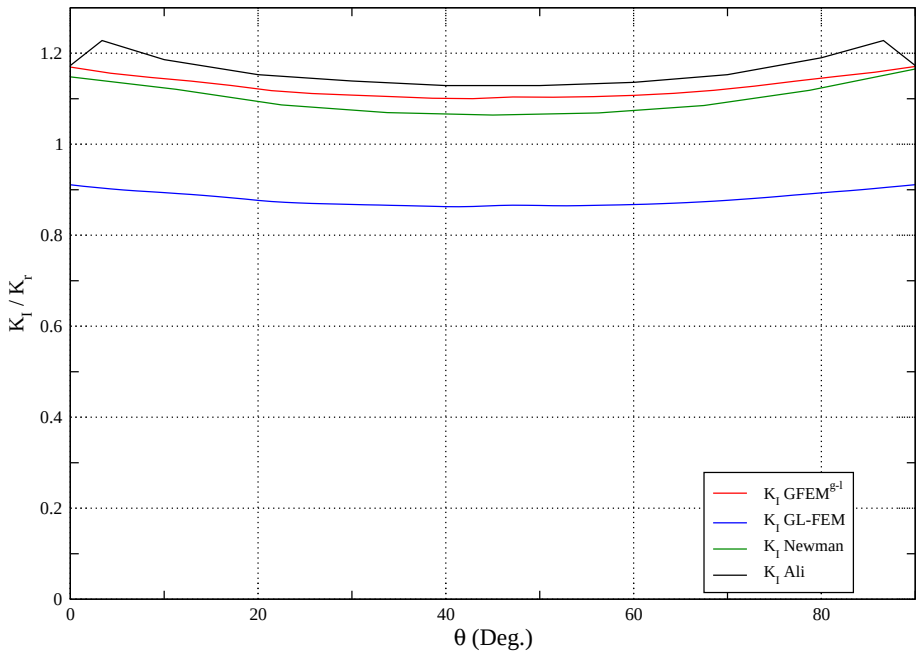

Fig. 10. Normalized mode I stress intensity factors for corner crack, $a/t = 0.2$.

Table 1. Size of the various discretizations in terms of number of degrees of freedom (DOFs).

Problem	Number of DOFs
Initial Global	10,170
Local	53,436
Enriched Global	10,290

Table 1 shows the size of the various discretizations used in the solution of this problem. The enriched global problem captures K_I very well while adding only 120 global-local enrichment degrees of freedom to the initial global problem. The computational cost of the local problem must also be considered in the total cost of the GFEM^{gl}. However, in most practical problems the global problem is much larger than the local one. Furthermore, the solution of the enriched global problem can be efficiently computed using the solution of the initial global problem [40, 25].

5.2.2. Three-dimensional crack propagation

In this section, we consider the fatigue crack growth simulation of the corner crack shown in Figure 8 using the GFEM^{gl}. The plate is subjected to cyclic uniaxial tension $\sigma(t)$ in the $x-$direction as illustrated in the figure. The magnitude of crack front advancement is computed using Paris-Erdogan equation [49]

$$\frac{da}{dN} = C\,(\Delta K)^m\,. \tag{14}$$

Parameters C and m are regarded as material constants, while $\Delta K = (1-R)K_{max}$ is the stress intensity factor range under cyclic loading, R is the ratio of minimum to maximum loads applied in a cycle and K_{max} is the stress intensity factor at the maximum load σ_{max}. The reader is referred to Section 4.2 of [50] for further details on the application of Equation (14) to compute crack front advance and fatigue life. The following parameters are adopted for the simulation presented in this section: $\sigma_{max} = 12\,MPa$, $R = 0$, $C = 0.0001$ and $m = 6$. Young's modulus and Poisson's ratio are taken as $E = 2000\,MPa$ and $\nu = 0.37$, respectively. The direction of crack front propagation is computed using stress intensity factors and Schöllmann's criterion

[51]. When $K_{III} = 0$, as in this example, this criterion is equivalent to the criterion of maximum tangential stress proposed by Erdogan and Sih [52].

The initial crack surface has an elliptical shape with major and minor radii a_0 and c_0, respectively. The following dimensions are adopted for the initial crack and plate (cf. Figure 8): $a_0/c_0 = 1.25$, $2h/c_0 = 224$, $a_0/t = 0.165$ and $a_0/b = 0.033$. Note that the initial crack is even smaller than the one used in the static case.

Similar to the case of static cracks, the propagating crack surface is not explicitly modeled in the global problem. Instead, it is represented through global-local enrichments. The initial local domain is defined by global elements contained in a bounding box with dimensions $bx/a_0 = 2$, $by/a_0 = 2$, $bz/a_0 = 2$. The size of the local domain increases during the simulation in order to accommodate the growing crack surface. The dimensions of the local domain are selected such that the ratios bx/a, by/a and bz/a remain close to 2. Figure 11 illustrates the local problem domains and their solutions at propagation steps 0, 30, 40, 60, 70, 83, 93, 103, 104 and 146.

It is important to mention that in the local domain mesh refinement is performed along the crack front. At the beginning of the simulation, it was adopted a ratio $L_e^L/a_0 \simeq 0.03$, where a_0 is the major axis of the initial crack surface. This ratio was kept approximately constant during the crack propagation simulation. Since the crack changes dramatically in size as it propagates, less mesh refinement is required to preserve the ratio L_e^L/a as the crack propagates. The localized refinement follows the crack front evolution using the refinement and unrefinement technique presented in [50]. On the other hand, in the enriched global domain the mesh remains unchanged throughout the entire crack growth simulation. The ratio between the size of the smallest element in the mesh of the global problem, L_e^G, and the minor axis of the initial crack, c_0 is $L_e^G/c_0 = 0.77$. This ratio is several times larger than what is required for acceptable accuracy in the FEM.

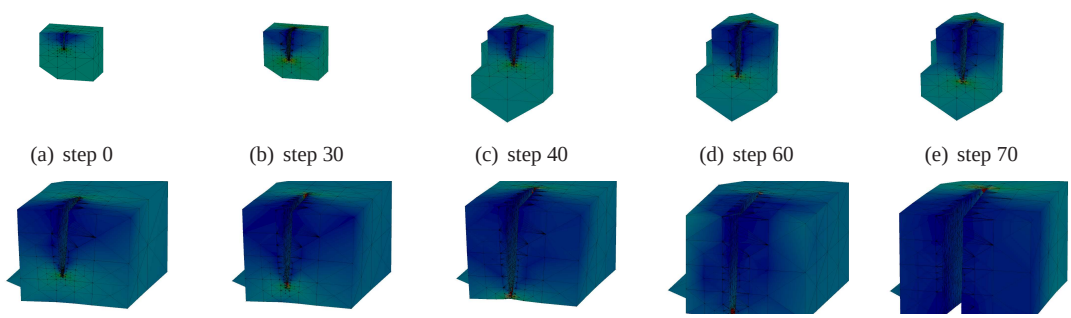

(a) step 0 (b) step 30 (c) step 40 (d) step 60 (e) step 70

(f) step 83 (g) step 93 (h) step 103 (i) step 104 (j) step 146

Fig. 11. Local problem domains and solutions at various crack growth steps. The size of the local domain increases during the simulation in order to accommodate the growing crack surface.

Figures 12 and 13 show the crack surface evolution at steps 0, 20, 35, 50, 70, 85, 93, 103, 110 and 146. It can be observed that at step 103 the crack front reaches the bottom surface of the plate and changes its topology. This type of transition is difficult to simulate using the FEM since the creation of strongly graded meshes fitting the crack surface while preserving the aspect ratio of the elements is not always possible in this case unless extremely small elements are used. In the GFEM^{gl} this can be handled without much difficulty by simply trimming the portion of the crack surface that may have advanced beyond the physical domain and snapping the crack front to the boundary of the domain. In addition, the global elements are orders of magnitude larger than those required by the FEM. Another challenge in this simulation is the significant change in size of the crack surface. This requires that the geometrical representation of the crack be adapted during the simulation. This process preserves a geometrically accurate representation of the crack front while reducing the number of facets at portions of the surface that are near flat or are far from the crack front.

Table 2 shows the size of the various discretizations used in the solution of this problem. In the table, “Initial Global Problem” corresponds to the uncracked global problem which has only polynomial

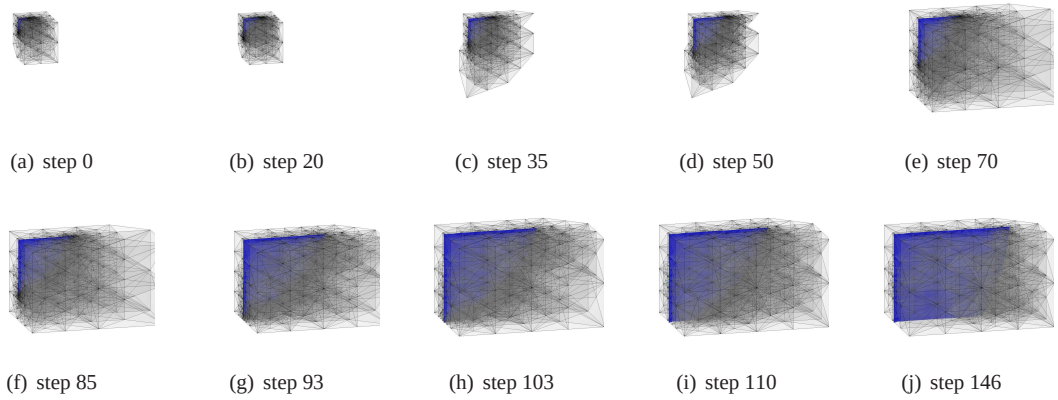

(a) step 0 (b) step 20 (c) step 35 (d) step 50 (e) step 70

(f) step 85 (g) step 93 (h) step 103 (i) step 110 (j) step 146

Fig. 12. *hp*-GFEM discretizations used at local domains. The local solutions are used as enrichments for the global problem.

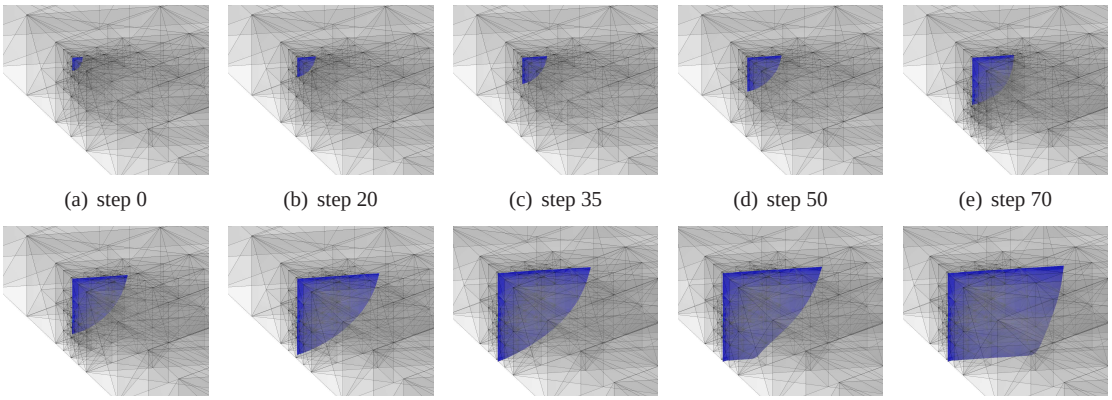

(a) step 0 (b) step 20 (c) step 35 (d) step 50 (e) step 70

(f) step 85 (g) step 93 (h) step 103 (i) step 110 (j) step 146

Fig. 13. Evolution of the crack surface in the enriched global problem. The global mesh is not refined during the simulation. The crack is approximated by global-local enrichments only. The crack surface changes topology around step 103 after the crack front reaches the bottom of the plate.

enrichments and no crack. The size of the problems changes as the crack grows. However, the number of global-local enrichments added to the initial global problem is at most 543, which is only 4.1% of the size of the uncracked global problem.

Table 2. Size of the various discretizations in terms of number of degrees of freedom (DOFs). The "Initial Global Problem" corresponds to the uncracked global problem which has only polynomial enrichments and no crack.

Problem	**Min. Number of DOFs**	**Max Number of DOFs**
Initial Global	13,110	13,110
Local	43,428	113,988
Enriched Global	13,310	13,653

5.3. Three-dimensional beam with localized plasticity

The scope of the GFEM^{gl}, as mentioned in Section 1, is not limited to linear elastic problems and it can be applied to problems involving non-linearities. The formulation of the GFEM^{gl} remains very similar to as described in Section 4. This section illustrates the effectiveness of the GFEM^{gl} in solving a three-

dimensional elasto-plastic mechanics problem with localized plasticity. Further details and specifics of the GFEM^{gl} for elasto-plastic problems are given in [34].

Figure 14 shows a bi-material cantilever beam subjected to a uniform traction in the vertical direction and magnitude $t_y = -1.50$, applied on the right-most face of the beam. The cross-section of the beam is 1×1. This figure also shows the global finite element mesh, a uniform mesh of $6*(10\times4\times4)$ tetrahedron elements, used to solve the problem, along with the boundary conditions which the beam is subjected to. This mesh was generated by first creating a $(10 \times 4 \times 4)$ structured mesh of hexahedral elements and then replacing each element by six tetrahedral elements. A cubic polynomial approximation is used for all elements in the mesh to capture bending of the beam accurately.

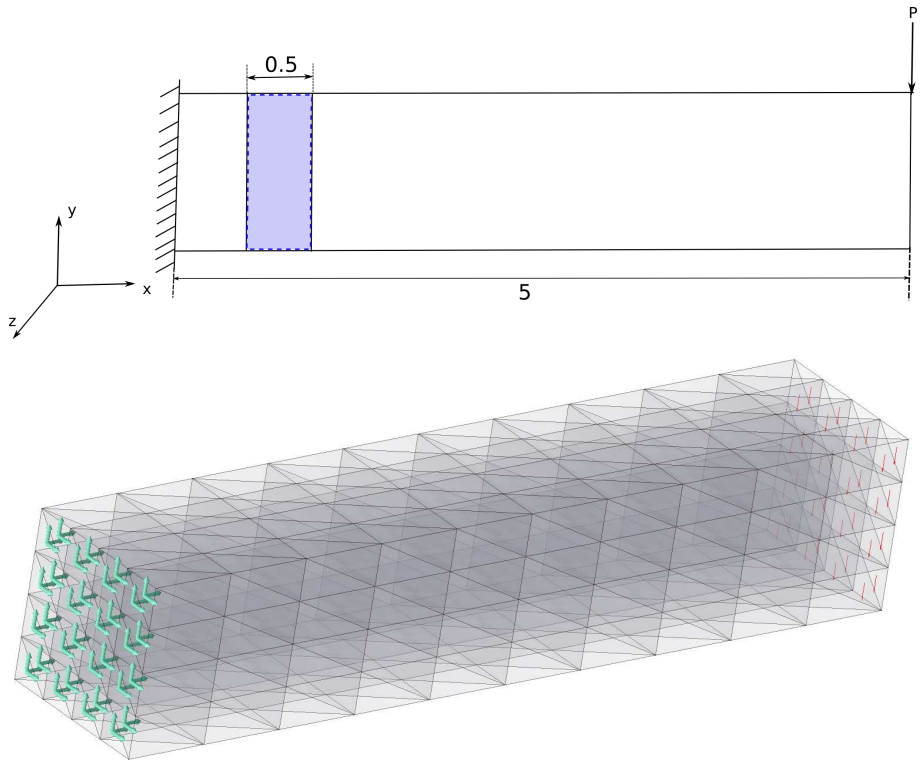

Fig. 14. A bi-material cantilever beam subjected to constant traction on the right end. The bottom figure features the finite element mesh with the boundary conditions applied. Green arrows on the left face represent the fixed displacement boundary conditions, and the red arrows on the right face represent the traction.

A linear isotropic hardening model is assumed to define the material properties for the beam, which are given in Table 3. The shaded region shown in Figure 14 has a lower initial yield stress ($\sigma_y = 15$) than the material in the rest of the beam. This will lead, for the load level considered in this problem, to a localized yielding in that layer of global elements. The material interfaces are located at element boundaries. The case of interfaces not fitting element boundaries can be handled by proper enrichment functions at local problems. An example of this class of functions is available at [53]. The relative norm of the residual is used as the tolerance criterion for the convergence of Newton-Raphson iterations, and the tolerance value is taken as 10^{-4}. A total of 30 uniform load steps are used to solve this nonlinear problem.

The procedure to analyze this problem using the GFEM^{gl}, as described in Section 4 is illustrated in Figure 15. The first step in this procedure involves the solution of the global problem on a coarse mesh with the full load applied and assuming a linear elastic material model. This problem is hereafter denoted as the *initial global problem*. A local domain, which fully contains the region with plastic strains, is then automatically extracted from this coarse global mesh as shown in the figure. The solution of the initial

Table 3. Material parameters of the isotropic hardening model used for the bi-material beam problem.

Material parameters	
Young's modulus (E)	7000
Poisson's ratio (ν)	0.20
Initial yield stress (σ_y)	70.0
Plastic Modulus (H)	500

global problem, obtained in the first step is used to prescribe boundary conditions for the local problem in the form of spring boundary conditions. The spring stiffness (κ) is selected based on Equation (9), and for this problem, a value of $\kappa = 14,000$ is used. The local problem is solved nonlinearly using Newton-Raphson iterations for the final load step with the assumption of linear isotropic hardening material model, given in Table 3. The computed nonlinear local solution is then used to enrich the global solution space at certain nodes in the coarse global mesh (shown as red spheres in Figure 15). This *enriched global problem* is then solved with the same nonlinear material model and a total of thirty uniform load steps.

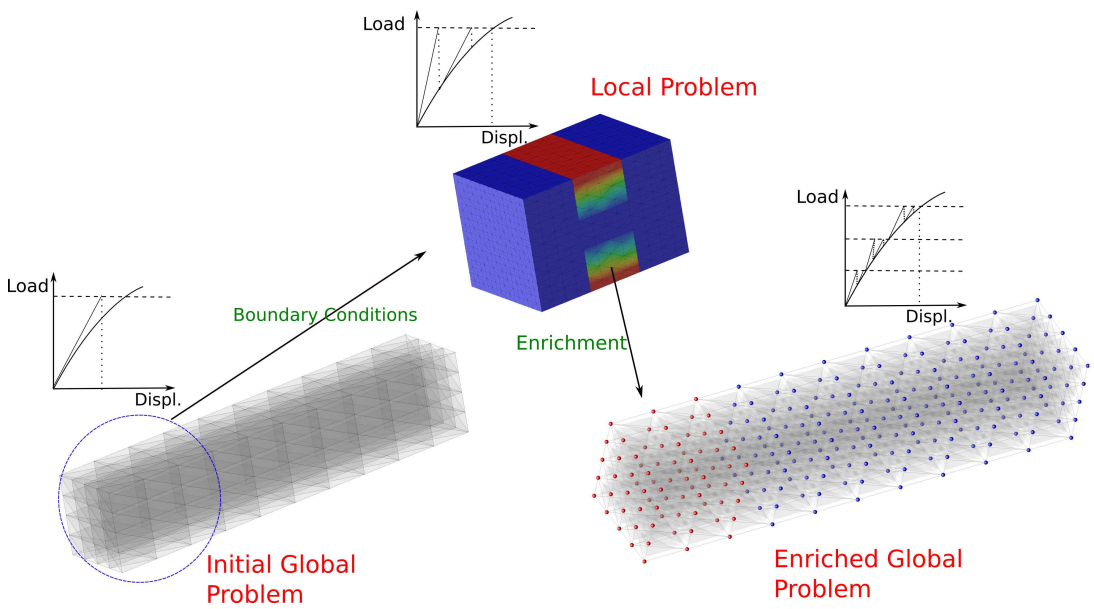

Fig. 15. Figure showing the algorithm for the nonlinear solution of the 3-D beam problem using GFEM^{gl}. Red nodes in the enriched global problem indicate nodes with global-local enrichments.

The reference solution to this problem is obtained using the *hp*-GFEM, which applies mesh refinement and enrichment to the global problem like in the standard *hp*-FEM [38] and is a very robust and efficient approach to capture fine scale behavior. The *hp*-GFEM discretization shown in Figure 17 uses the same element size h and polynomial order p as those selected for the local problem in the case of GFEM^{gl}. Figures 16 and 17 show the contour plots of the distribution of the norm of plastic strain tensor

$$\|\boldsymbol{\varepsilon}^p\| = \sqrt{{\varepsilon^p_{xx}}^2 + {\varepsilon^p_{yy}}^2 + {\varepsilon^p_{zz}}^2 + {\varepsilon^p_{xy}}^2 + {\varepsilon^p_{yz}}^2 + {\varepsilon^p_{zx}}^2} \tag{15}$$

obtained with the GFEM^{gl} and *hp*-GFEM, respectively. This norm is equivalent to the Frobenius norm of a second order tensor. As can be seen from the figures, the plastic strain distribution in the two cases are very similar, in spite of using a coarse global mesh in the case of GFEM^{gl}. Figure 18 shows the distribution of the norm of plastic strain tensor for the GFEM solution obtained by solving the problem on the coarse

global mesh, i.e., without $h-$refinement in the region with localized plasticity. The plastic strain distribution is clearly not well captured by this discretization.

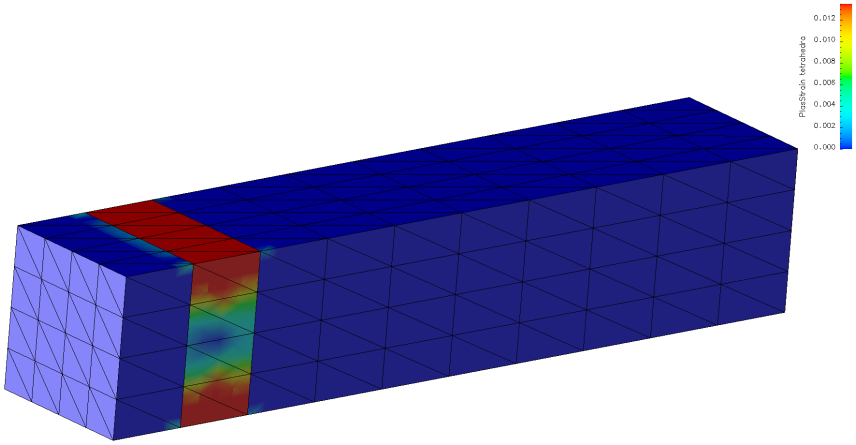

Fig. 16. Figure showing the distribution of the norm of plastic strain tensor in the case of GFEM^{gl}.

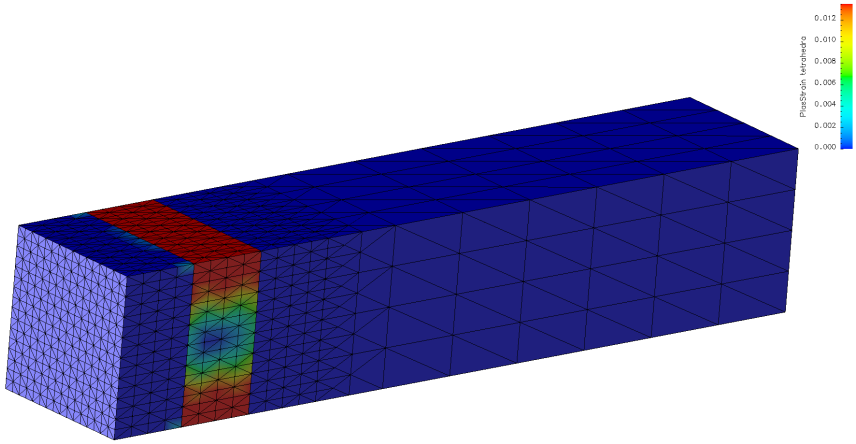

Fig. 17. Figure showing the distribution of the norm of plastic strain tensor in the case of *hp*-GFEM.

Figure 19 shows the plot of the $y-$displacement component at the centroid of the extreme right face of the beam against the load step for the three discretizations described above. The non-linear response of the problem is quite evident from this plot and shows that the GFEM^{gl} solution agrees very well with that of *hp*-GFEM. Even though, the $y-$displacement, which is a global response quantity, obtained from the GFEM solution on a coarse finite element mesh is not too far from the reference solution, the local distribution of plastic strains is significantly different, as seen from figures 16, 17 and 18. Therefore, a coarse finite element model is not suitable for predicting, for example, a localized failure of the beam. In contrast, the local distribution of plastic strains predicted by the GFEM^{gl} approach is clearly close to the reference solution (*hp*-GFEM solution).

Table 4 lists the number of DOFs corresponding to each of the three discretizations used to solve this problem. The GFEM^{gl} captures the global and localized responses very well with just the addition of $225(= 8475-8250)$ degrees of freedom to the coarse global mesh. The *hp*-GFEM discretization, in contrast, requires many more degrees of freedom to achieve comparable accuracy.

Table 5 lists the number of Newton-Raphson iterations at each load step for the cases of GFEM^{gl} and *hp*-GFEM. The problem behaves linearly up to 11th load step, and thereby leading to just one iteration in the

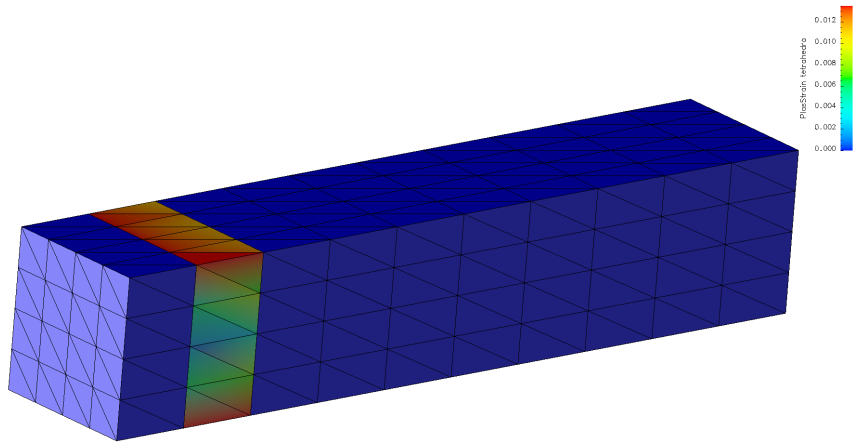

Fig. 18. Figure showing the distribution of the norm of plastic strain tensor in the case of GFEM on a coarse global mesh *not* enriched with global-local functions.

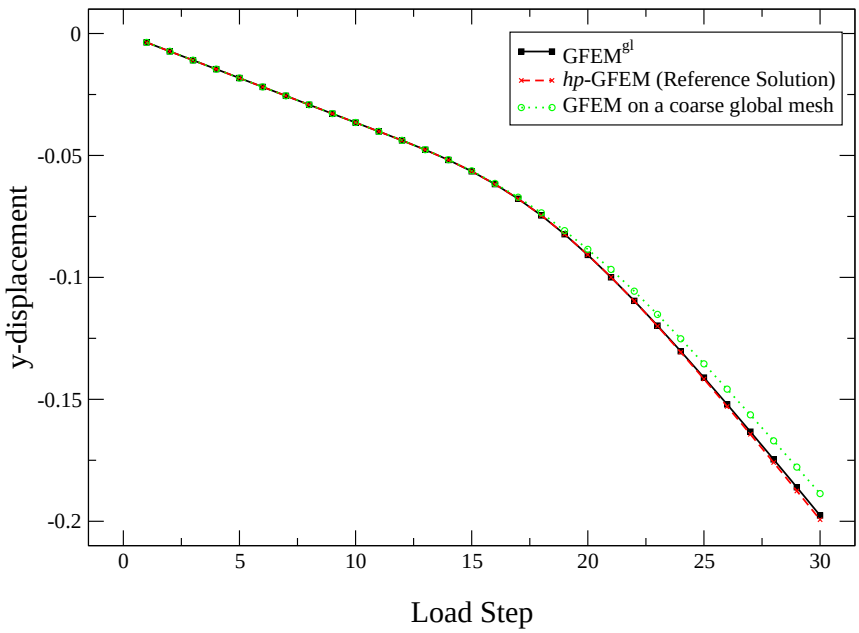

Fig. 19. Plot of *y*-displacement at the centroid of the extreme right face of the beam against the load step.

Table 4. Size of the problem in terms of number of degrees of freedom (DOFs) for different methods.

Method	Number of DOFs
GFEM with a coarse mesh	8250
GFEM^{gl}	8475
hp-GFEM	126,630

first 11 load steps. From this table, it can be seen that the GFEM^{gl} takes equal or lesser number of iterations at each load step as when compared to *hp*-GFEM. Since the GFEM^{gl} discretization has significantly fewer DOFs than the *hp*-GFEM and the local problem is solved only once, we can conclude that the computational cost of the GFEM^{gl} is lower than that of the *hp*-GFEM.

Table 5. Number of Newton-Raphson iterations to solve the nonlinear beam problem.

Load step	Number of iterations	
	hp-GFEM	GFEM^{gl}
11	1	1
12	5	3
13	4	4
14	5	4
15	4	4
16	5	4
17	4	4
18	4	4
19	5	4
20	5	4
21	4	4
22	5	4
23	5	4
24	4	4
25	5	4
26	5	4
27	7	4
28	5	4
29	5	4
30	7	4

6. Conclusions

The examples presented in Section 5.2 demonstrate that the GFEM^{gl} is able to simulate three-dimensional fracture mechanics problems using global discretizations with elements that are orders of magnitude larger than those required by the FEM. This leads to global problems of much reduced dimension than in the FEM. The computational cost of the GFEM^{gl} can be further reduced. In this paper a single local problem is defined, for example, at each crack propagation step. However, a local problem can be defined for each node of the coarse-scale mesh whose partition of unity support intersects the crack surface. These local problems can be efficiently solved in parallel, since *no communication among processors solving different local problems is required* [54]. This leads to very scalable computations even on shared memory machines [54].

This paper also demonstrates that the GFEM^{gl} is not limited to linear problems. A problem involving a non-linear material response is solved to demonstrate this. It is shown that the GFEM^{gl} is able to capture details of non-linear strain fields using coarse meshes. The example presented in Section 5.3 also demonstrates that the GFEM^{gl} takes equal or lesser number of Newton iterations at each load step as when compared to available discretization approaches. This translates into a reduced computational cost for the method.

While not explored in this paper, it is conceivable to combine the GFEM^{gl} with the GFEM for polycrystals described in Section 3. This would enable the discretization of polycrystalline micro-structures at the local problems while keeping the global discretization coarse. This and other similar ideas are currently being investigated by our groups.

Acknowledgments: The support from the U.S. Air Force Office of Scientific Research under contract number FA9550-09-1-0401 (C.A. Duarte and V. Gupta) is gratefully acknowledged.

References

[1] J. Oden, T. Belytschko, I. Babuška, T. Hughes, Research directions in computational mechanics, Computer Methods in Applied Mechanics and Engineering 192 (2003) 913–922.

[2] T. Beberniss, T. Eason, B. Gordon, M. Haney, J. Hollkamp, M. Spottswood, Response prediction for structures in extreme environments, Tech. rep., Structural Science Center, AFRL/VASM (2007).

[3] H. Simon, T. Zacharia, R. Stevens, Modeling and simulation at the exascale for energy and the environment, Tech. rep., Lawrence Berkeley National Laboratory (2007).

[4] R. Bank, L. Scott, On the conditioning of finite element equations with highly refined meshes, SIAM Journal on Numerical Analysis.

[5] I. Babuška, J. Melenk, The partition of unity finite element method, Tech. Rep. BN-1185, Inst. for Phys. Sc. and Tech., University of Maryland (Jun. 1995).

[6] I. Babuška, J. Melenk, The partition of unity method, International Journal for Numerical Methods in Engineering 40 (1997) 727–758.

[7] C. Duarte, I. Babuška, J. Oden, Generalized finite element methods for three dimensional structural mechanics problems, Computers and Structures 77 (2000) 215–232.

[8] J. Oden, C. Duarte, O. Zienkiewicz, A new cloud-based *hp* finite element method, Computer Methods in Applied Mechanics and Engineering 153 (1998) 117–126.

[9] T. Strouboulis, K. Copps, I. Babuška, The generalized finite element method, Computer Methods in Applied Mechanics and Engineering 190 (2001) 4081–4193.

[10] I. Babuška, G. Caloz, J. Osborn, Special finite element methods for a class of second order elliptic problems with rough coefficients, SIAM Journal on Numerical Analysis 31 (4) (1994) 945–981.

[11] J. Melenk, I. Babuška, The partition of unity finite element method: Basic theory and applications, Computer Methods in Applied Mechanics and Engineering 139 (1996) 289–314.

[12] C. Duarte, J. Oden, Hp clouds–A meshless method to solve boundary-value problems, Tech. Rep. 95-05, TICAM, The University of Texas at Austin (May 1995).

[13] C. Duarte, J. Oden, An *hp* adaptive method using clouds, Computer Methods in Applied Mechanics and Engineering 139 (1996) 237–262.

[14] C. Duarte, J. Oden, *Hp* clouds – An *hp* meshless method, Numerical Methods for Partial Differential Equations 12 (1996) 673–705.

[15] C. Duarte, *The hp Cloud Method*, PhD dissertation, The University of Texas at Austin, austin, TX, USA (December 1996).

[16] N. Moës, J. Dolbow, T. Belytschko, A finite element method for crack growth without remeshing, International Journal for Numerical Methods in Engineering 46 (1999) 131–150.

[17] T. Belytschko, T. Black, Elastic crack growth in finite elements with minimal remeshing, International Journal for Numerical Methods in Engineering 45 (1999) 601–620.

[18] T. Belytschko, R. Gracie, G. Ventura, A review of extended/generalized finite element methods for material modeling, Modelling and Simulations in Materials Science and Engineering 17 (2009) 24pp, http://dx.doi.org/10.1088/0965-0393/17/4/043001.

[19] T.-P. Fries, T. Belytschko, The generalized/extended finite element method: An overview of the method and its applications, International Journal for Numerical Methods in Engineering (2010) 253–304.

[20] A. Simone, C. Duarte, E. van der Giessen, A generalized finite element method for polycrystals with discontinuous grain boundaries, International Journal for Numerical Methods in Engineering 67 (8) (2006) 1122–1145. doi:10.1002/nme.1658.

[21] C. Felippa, Introduction to finite element methods., course Notes. Department of Aerospace Engineeing Sciences, University of Colorado at Boulder. Available at http://www.colorado.edu/engineering/Aerospace/CAS/courses.d/IFEM.d (2004).

[22] A. Noor, Global-local methodologies and their applications to nonlinear analysis, Finite Elements in Analysis and Design 2 (1986) 333–346.

[23] J. Whitcomb, Iterative global/local finite element analysis, Computers and Structures 40 (1991) 1027–1031.

[24] I. Hirai, B. Wang, W. Pilkey, An efficient zooming method for finite element analysis, International Journal for Numerical Methods in Engineering 20 (1984) 1671–1683.

[25] J. Pereira, D.-J. Kim, C. Duarte, A two-scale approach for the analysis of propagating three-dimensional fractures, Computational MechanicsAccepted for publication. doi:10.1007/s00466-011-0631-4.

[26] S. Loehnert, T. Belytschko, A multiscale projection method for macro/microcrack simulations, International Journal for Numerical Methods in Engineering 71 (12) (2007) 1466–1482.

[27] E. Chahine, P. Laborde, Y. Renard, Spider-xfem, an extended finite element variant for partially unknown crack-tip displacement, European Journal of Computational Mechanics 15 (5-7) (2008) 625–636.

[28] E. Chahine, P. Laborde, Y. Renard, A reduced basis enrichment for the extended finite element method, Mathematical Modelling of Natural Phenomena 4 (1) (2009) 88–105.

[29] A. Menk, P. Bordas, Numerically determined enrichment functions for the extended finite element method and applications to bi-material anisotropic fracture and polycrystals, International Journal for Numerical Methods in Engineering 83 (7) (2010) 805828.

[30] S. Mousavi, E. Grinspun, N. Sukumar, Harmonic enrichment functions: A unified treatment of multiple, intersecting and branched cracks in the extended finite element method, International Journal for Numerical Methods in Engineering 85 (2011) 13061322. doi:10.1002/nme.3020.

[31] D.-J. Kim, C. Duarte, J. Pereira, Analysis of interacting cracks using the generalized finite element method with global-local enrichment functions, Journal of Applied Mechanics 75 (5) (2008) 051107. doi:10.1115/1.2936240.

[32] P. O'Hara, C. Duarte, T. Eason, Generalized finite element analysis of three-dimensional heat transfer problems exhibit-

ing sharp thermal gradients, Computer Methods in Applied Mechanics and Engineering 198 (21-26) (2009) 1857–1871. doi:10.1016/j.cma.2008.12.024.

[33] P. O'Hara, C. Duarte, T. Eason, Transient analysis of sharp thermal gradients using coarse finite element meshes, Computer Methods in Applied Mechanics and Engineering 200 (5-8) (2011) 812–829. doi:10.1016/j.cma.2010.10.005.

[34] D.-J. Kim, C. Duarte, S. Proenca, A generalized finite element method with global-local enrichment functions for confined plasticity problems, Computational MechanicsSubmitted.

[35] V. Gupta, D.-J. Kim, C. Duarte, Analysis and improvements of the global-local enrichment functions for the generalized finite element method, Computer Methods in Applied Mechanics and EngineeringTo be submitted.

[36] C. Duarte, D.-J. Kim, Analysis and applications of a generalized finite element method with global-local enrichment functions, Computer Methods in Applied Mechanics and Engineering 197 (6-8) (2008) 487–504. doi:10.1016/j.cma.2007.08.017.

[37] K. Tanaka, Mechanics and micromechanics of fatigue crack propagation, in: R. Wei, R. Gangloff (Eds.), Fracture Mechanics: Perspectives and Directions (Twentieth Symposium), ASTM STP 1020, American Society for Testing and Materials, Philadelphia, 1989, pp. 151–183.

[38] B. Szabo, I. Babuška, Finite Element Analysis, John Wiley and Sons, New York, 1991.

[39] J. Pereira, C. Duarte, D. Guoy, X. Jiao, *Hp*-Generalized FEM and crack surface representation for non-planar 3-D cracks, International Journal for Numerical Methods in Engineering 77 (5) (2009) 601–633. doi:10.1002/nme.2419.

[40] D.-J. Kim, J. Pereira, C. Duarte, Analysis of three-dimensional fracture mechanics problems: A two-scale approach using coarse generalized FEM meshes, International Journal for Numerical Methods in Engineering 81 (3) (2010) 335–365. doi:10.1002/nme.2690.

[41] X.-P. Xu, A. Needleman, Numerical simulations of fast crack growth in brittle solids, Journal of the Mechanics and Physics of Solids 42 (9) (1994) 1397–1434.

[42] C. Duarte, L. Reno, A. Simone, A high-order generalized FEM for through-the-thickness branched cracks, International Journal for Numerical Methods in Engineering 72 (3) (2007) 325–351. doi:10.1002/nme.2012.

[43] Z. Shabir, E. V. der Giessen, C. A. Duarte, A. Simone, The role of cohesive properties on intergranular crack propagation in brittle polycrystals, Modelling and Simulation in Materials Science and Engineering 19 (3) (2011) 035006. doi:10.1088/0965-0393/19/3/035006.

[44] J. Raju, I.S. Newman Jr., Finite-element analysis of corner cracks in rectangular bars, Tech. rep., NASA (1987).

[45] O. A. Ali, Mixed mode stress intensity factors for deflected and inclined corner cracks in finite-thickness plates, International Journal of Fracture 29 (2007) 305–317.

[46] J. Pereira, C. Duarte, Computation of stress intensity factors for pressurized cracks using the generalized finite element method and superconvergent extraction techniques, in: P. Lyra, S. da Silva, F. Magnani, L. do N. Guimaraes, L. da Costa, E. P. Junior (Eds.), XXV Iberian Latin-American Congress on Computational Methods in Engineering, Recife, PE, Brazil, 2004, 15 pages. ISBN Proceedings CD: 857 409 869-8.

[47] J. Pereira, C. Duarte, Extraction of stress intensity factors from generalized finite element solutions, Engineering Analysis with Boundary Elements 29 (2005) 397–413.

[48] J. Pereira, C. Duarte, The contour integral method for loaded cracks, Communications in Numerical Methods in Engineering 22 (5) (2006) 421–432. doi:10.1002/cnm.824.

[49] A. Paris, F. Erdogan, A critical analysis of crack propagation laws, Journal of Basic Engineering 85 (1963) 528–534.

[50] J. Pereira, C. Duarte, X. Jiao, Three-dimensional crack growth with *hp*-generalized finite element and face offsetting methods, Computational Mechanics 46 (3) (2010) 431–453. doi:10.1007/s00466-010-0491-3.

[51] M. Schöllmann, H. Richard, G. Kullmer, M. Fulland, A new criterion for the prediction of crack development in multiaxially loaded structures, International Journal of Fracture 117 (2002) 129–141.

[52] F. Erdogan, G. Sih, On the crack extension in plates under plane loading and transverse shear, Journal of Basic Engineering 85 (1963) 519–525.

[53] A. Aragon, C. Duarte, P. Geubelle, Generalized finite element enrichment functions for discontinuous gradient fields, International Journal for Numerical Methods in Engineering 82 (2) (2010) 242–268. doi:10.1002/nme.2772.

[54] D.-J. Kim, C. Duarte, N. Sobh, Parallel simulations of three-dimensional cracks using the generalized finite element method, Computational Mechanics 47 (3) (2011) 265–282. doi:10.1007/s00466-010-0546-5.